

ORIGINAL ARTICLE

Processing of Egomotion-Consistent Optic Flow in the Rhesus Macaque Cortex

Benoit R. Cottetereau^{1,2}, Andrew T. Smith³, Samy Rima^{1,2}, Denis Fize⁴, Yseult Héjja-Brichard^{1,2}, Luc Renaud^{5,6}, Camille Lejards^{1,2}, Nathalie Vayssiére^{1,2}, Yves Trotter^{1,2} and Jean-Baptiste Durand^{1,2}

¹Université de Toulouse, Centre de Recherche Cerveau et Cognition, Toulouse, France, ²Centre National de la Recherche Scientifique, Toulouse, France, ³Department of Psychology, Royal Holloway, University of London, Egham, UK, ⁴Laboratoire d'Anthropologie Moléculaire et Imagerie de Synthèse, CNRS-Université de Toulouse, Toulouse, France, ⁵CNRS, CE2F PRIM UMS3537, Marseille, France and ⁶Aix Marseille Université, Centre d'Exploration Fonctionnelle et de Formation, Marseille, France

Address correspondence to Benoit R. Cottetereau and Jean-Baptiste Durand, CNRS CERCO UMR 5549, Pavillon Baudot, CHU Purpan, BP 25202, 31052 Toulouse Cedex, France. Email: cottetereau@cerco.ups-tlse.fr (B.R.C.); jbdurand@cnrs.fr (J.-B.D.)

Abstract

The cortical network that processes visual cues to self-motion was characterized with functional magnetic resonance imaging in 3 awake behaving macaques. The experimental protocol was similar to previous human studies in which the responses to a single large optic flow patch were contrasted with responses to an array of 9 similar flow patches. This distinguishes cortical regions where neurons respond to flow in their receptive fields regardless of surrounding motion from those that are sensitive to whether the overall image arises from self-motion. In all 3 animals, significant selectivity for egomotion-consistent flow was found in several areas previously associated with optic flow processing, and notably dorsal middle superior temporal area, ventral intra-parietal area, and VPS. It was also seen in areas 7a (Opt), STPm, FEFsem, FEFsac and in a region of the cingulate sulcus that may be homologous with human area CSv. Selectivity for egomotion-compatible flow was never total but was particularly strong in VPS and putative macaque CSv. Direct comparison of results with the equivalent human studies reveals several commonalities but also some differences.

Key words: egomotion, heading, monkey fMRI, optic flow, vision

Introduction

In macaques, numerous regions of the cerebral cortex contain at least some neurons that are selectively responsive to the direction of motion of a moving visual stimulus. These regions have diverse locations including large parts of the occipital cortex, posterior portions of the temporal cortex, the inferior parietal cortex, and even parts of the frontal cortex. Although the most obvious use of sensitivity to image motion is to specify the

motion of external objects, it is also valuable for monitoring the animal's own movements. Two cortical regions in particular, the dorsal middle superior temporal area (MSTd) and the ventral intra-parietal area (VIP), are associated with the specialized function of encoding visual cues to self-motion. Both contain many neurons that are selectively sensitive to specific components of the optic flow that occurs during self-motion, including direction of heading during locomotion (Tanaka et al. 1989;

Duffy and Wurtz 1991, 1995; Bremmer et al. 2002a). Electrical stimulation of these regions can influence heading judgments (Britten and van Wezel 2002; Zhang and Britten 2011) suggesting that they contribute directly to perceptual awareness of self-motion, although this has recently been questioned in the case of VIP (Chen et al. 2016). Many MSTd and VIP neurons also receive vestibular input (Duffy et al. 1976; Gu et al. 2006; Chen et al. 2011a) and there is evidence that visual and vestibular cues are efficiently integrated by such neurons, with weightings based on cue reliability (Fetsch et al. 2012). Neurons that appear to encode optic flow have also been identified in area 7a of the inferior parietal lobule (Motter and Mountcastle 1981; Steinmetz et al. 1987) and recently in the frontal eye fields (Gu et al. 2015), where again many neurons also respond to vestibular stimuli.

Despite much research, it is not known exactly how visual responses to specific types of optic flow are constructed. The problem has proved challenging and although several sophisticated and biologically plausible models have been proposed (e.g., Perrone and Stone 1994; Grossberg et al. 1999; Yu et al. 2010; Mineault et al. 2012), the computations involved are still debated. However, it is clear that signals encoding motion, which is initially encoded locally, must be spatially integrated in some way. By definition, self-motion generates full-field visual stimulation: When the animal moves, the entire retinal image moves. Receptive fields in MSTd and VIP are large enough (typically 10–50 degs, e.g., Komatsu and Wurtz 1988; Schaafsma and Duyens 1996; Mendoza-Halliday et al. 2014) to integrate local motion signals over a wide area, and in some cases a significant proportion of the visual field, but they are not large enough to integrate signals over the entire visual field. The question therefore arises: Do the responses of flow-selective neurons having different receptive field locations combine to specify the overall optic flow, and if so how? Visual responses are usually studied with a simulated optic flow stimulus positioned such that all key features of the flow are contained within the receptive field. For example, in the case of expansion (forward motion), the center of expansion is typically placed within the receptive field being examined. The implicit assumption is that single neurons are concerned with optic flow only within their receptive fields and can therefore be expected to respond the same way to a given stimulus irrespective of whether the remainder of the visual field is consistent with the same optic flow. However, this has not been tested empirically and consequently we do not know whether neurons in MST and VIP respond 1) whenever what falls in their purview “could be” part of full-field optic flow, or 2) only, or at least more strongly, when signals from other parts of the visual field indicate that it actually is part of full-field flow. Whether MSTd and VIP encode optic flow per se, or localized flow components that can be used to derive overall optic flow, is a key unanswered question.

Surprisingly, perhaps, the above question has been better addressed in humans than in macaques. In the human brain, putative homologs of macaque MST (Dukelow et al. 2001; Huk et al. 2002; Kolster et al. 2010) and VIP (Bremmer et al. 2001) have been identified. These have been shown to be involved in encoding optic flow (Smith et al. 2006; Cardin et al. 2012a). Wall and Smith (2008) addressed the question of whether human MST (hMST) and VIP are active whenever optic flow components are present in the image, or only when full-field flow is present. They presented an array of 9 (3 × 3) optic flow patches. The patches were identical and each contained spiraling flow that would be expected to provide a good stimulus for a macaque MST neuron if presented in its receptive field. However, the array

as a whole was not consistent with self-motion and should not activate neurons that respond selectively to image motion caused by self-motion. Wall and Smith (2008) found that hMST responded almost as strongly to the array as to a single large patch of the same total size, suggesting that it is not strongly sensitive to whether or not image motion reflects self-motion. In putative human VIP, the response was about half that to a single patch, implying stronger selectivity for self-motion. A more extensive study using the same paradigm (Cardin and Smith 2010) confirmed these findings and additionally identified 2 more visually responsive regions that respond at least twice as well to one patch as to an array. One was human V6 (hV6), a region identified in humans only quite recently (Pitzalis et al. 2006) and thought to be the homologue of macaque V6 (Galletti et al. 2001). The other was labeled PIVC (parieto-insular vestibular cortex) but was probably PIC (posterior insular cortex), a visual-vestibular region immediately posterior to human PIVC (Frank et al. 2014) that may be homologous to macaque VPS (visual posterior sylvian area; Chen et al. 2011b). In macaques, both V6 (Fan et al. 2015) and VPS (Chen et al. 2011b) contain neurons that are tuned for visually simulated direction of heading. In both the above human fMRI (functional magnetic resonance imaging) studies (Wall and Smith 2008; Cardin and Smith 2010), the strongest specificity to visual self-motion occurred in a region not previously studied in any detail, the cingulate sulcus visual (CSV) area. Here, a strong response could be elicited by a single optic flow patch but the response was almost completely abolished when an array of optic flow patches was used as substitute. Recent studies (Antal et al. 2008; Fischer et al. 2012) confirm the role of CSV in self-motion processing and an additional piece of evidence implicating CSV in self-motion processing is that it receives vestibular as well as visual input (Smith et al. 2012). Thus, population responses in human visual cortex show a hierarchy of sensitivity to whether the overall visual image is likely to reflect self-motion, from hMST (weakest sensitivity), through hV6 and hVIP (substantial sensitivity), to PIC and CSV (strongest sensitivity).

There have been no single-unit studies in macaques that used either the multi-patch approach or, to our knowledge, any other approach to distinguish responses to true, full-field optic flow from responses to the mere presence of optic flow segments in the receptive field. Before undertaking such studies, it would be valuable to establish with fMRI which macaque visual areas, if any, show such differentiation on a macroscopic scale. This would guide physiological experimentation and also provide a much stronger link with the relevant human fMRI literature. There are numerous important species differences that could make human fMRI studies an unreliable guide to macaque physiology. Not least, area CSV has not been identified in macaques. We have therefore employed the multi-patch paradigm during fMRI in alert fixating macaques with the aim of establishing candidate visual regions for true self-motion specialization, in the sense discussed above.

Materials and Methods

Animal Model

Subjects

Three female rhesus macaques: M01, M02, and M03 (age: 5–7 years; weight: 4.5–6.5 kg) were involved in this study. Animal housing, handling, and all experimental protocols (surgery, behavioral training, and MRI (magnetic resonance imaging) recordings) followed the guidelines of the European Union legislation (2010/63/UE) and of the French Ministry of Agriculture

(décret 2013-118). The project was approved by a local ethics committee (CNREEA code: C2EA – 14) and received authorization from the French Ministry of Research (MP/03/34/10/09). The 3 animals were housed together in a large, enriched enclosure and could thus develop social and foraging behaviors. They returned to their individual cages to be fed twice a day, with standard primate biscuits supplemented with various types of fruits and vegetables. Health inspections were carried out quarterly on these animals. Details about the animals' surgical preparation and behavioral training are provided as Supplementary text 1.

Optic Flow Stimuli

The stimuli were identical to those used in previous human studies (Wall and Smith 2008; Cardin and Smith 2010). They consisted of 800 moving dots arranged in an egomotion-consistent (EC) or egomotion-inconsistent (EI) pattern. The EC condition consisted of a $40^\circ \times 40^\circ$ square field of dots moving in a coherent optic flow pattern containing expansion/contraction and rotation components that varied over time, consistent with self-motion on a varying spiral trajectory (Morrone et al. 2000), displayed at 60 fps. For a given dot with radius r , angle θ , and local speed v , its trajectory was defined by:

$$\frac{dr}{dt} = v \cos \phi$$

$$\frac{d\theta}{dt} = (v \sin \phi)/r$$

Radial and angular velocities are defined by dr/dt and $d\theta/dt$, respectively. The direction of optic flow was defined by ϕ , which varied over time from $-\pi$ to π generating stimuli with radial, circular, and spiral motion. The EI stimulus consisted of a 3×3 array of 9 identical panels, each containing a smaller version of the EC stimulus. Although the individual panels contain optic flow, the overall pattern is not consistent with egomotion because flow induced by observer motion can have only one center of motion. In true optic flow stimuli, the size and speed of motion of the features in the image increase with eccentricity. Because the introduction of these scaling factors would result in different distributions of dot size and speed in our 2 stimuli, and potentially spurious results, we kept the dot size, dot speed, and number of dots in the whole array identical across conditions in order to equate low-level visual characteristics. As a result, our stimulus does not accurately simulate "true" optic flow in terms of the scaling of size and speed with eccentricity typical of motion through a cloud of dots. The use of time-varying flow ensured that all locations were stimulated by all dot directions during the course of the stimulus cycle. It also provides larger responses than continuous expansion because multiple flow-sensitive neurons are stimulated. Finally, it ensures that adaptation at any one local direction is minimal.

MRI Recordings

Images were acquired on a 3 Tesla clinical MR scanner (Phillips Achieva) using a custom 8-channel phased array coil (RapidBiomed) specially designed to fit the skull of macaques while preserving their field of view.

Recordings for Individual Templates

For each individual, anatomical, and functional brain templates were built from acquisitions made in a single session on slightly anaesthetized animals (Zoletil 100:10 mg/kg and

Domitor: 0.04 mg/kg). The animals' constants were monitored during the whole session (about 1 h) with an MR compatible oximeter. During that session, we acquired 4 T1-weighted anatomical volumes magnetization prepared rapid gradient echo (MPRAGE; repetition time [TR] = 10.3 ms; echo time [TE] = 4.6 ms, flip angle = 8° ; voxel size = $0.5 \times 0.5 \times 0.5$ mm; 192 slices), and 300 functional volumes (GE-EPI; TR = 2000 ms, TE = 30 ms, flip angle = 90° , SENSE factor = 1.6; voxel size = $1.25 \times 1.25 \times 1.5$ mm, 32 axial slices).

Recordings for Functional Sessions

The functional scanning sessions were performed on awake behaving animals on a daily basis and lasted for about 1 h (8–12 runs). The animals were head-fixed, seated in a sphynx position within their primate chair (Fig. 1A). They were introduced into the bore of the magnet, facing a translucent screen at a distance of 50 cm. Visual stimuli were rear-projected on the screen by a video projector (Hitachi, CP_X809), at a spatial resolution of 1024×768 pixels and a refresh rate of 60 Hz. The position of one eye was monitored with an infrared video-based eye-tracker at 60 Hz (ASL). Functional images were acquired with the same GE-EPI sequence as that used during the anesthetized sessions. EC and EI stimuli were presented using a block-design. Each run consisted of 224 s (112 TRs) divided into 7 identical cycles of 32 s (16 TRs). In half of the runs, a cycle started with a baseline of 10 s (5 TRs) where only the fixation point was present. It was followed by 6 s (3 TRs) of the EC condition, then by another 10 s of blank and finally by 6 s of the EI condition (Fig. 1B). In the other half of the runs, the EC and EI conditions were reversed within a cycle (i.e., a cycle had 10 s of blank, 6 s of the EI condition, 10 s of blank, and finally 6 s of the EC condition). Video display and reward for correct fixation were controlled using the V-Cortex software.

Data Processing

Anatomical and Functional Templates

Data collected during the anesthetized sessions were used to compute individual functional and anatomical templates. The anatomical template was obtained by realigning and averaging the 4 T1-weighted (MPRAGE) volumes. It was then aligned to the MNI space of the 112RM-SL template (McLaren et al. 2009, 2010). Cortical surface reconstruction were performed using the CARET software (Van Essen et al. 2001). The functional template was obtained by realigning and averaging the 300 functional (GE-EPI) volumes. It was aligned with the anatomical template and spatial normalization parameters (affine and non-rigid) between the functional and anatomical templates were determined based on the gray matter maps of both templates. For group analyses, the same operation was performed to register each individual anatomical template to the F99 template available in the CARET software (Van Essen 2002).

Preprocessing of the Functional Data

In total, 36 runs per animal were kept for further analyses (18 runs with the EC condition first during the blocks and 18 runs with the EI condition first). All those runs were selected based on the quality of fixation (percentage of correct fixation >85%) in order to minimize the influence of eye movements in blood-oxygen-level dependant (BOLD) signal fluctuations (see Supplementary text 2 and Supplementary Fig. 1 for an additional control on the influence of eye position on our results). Within each run, volumes were rigidly realigned with each other on a slice-by-slice basis using a subpixel cross-correlation

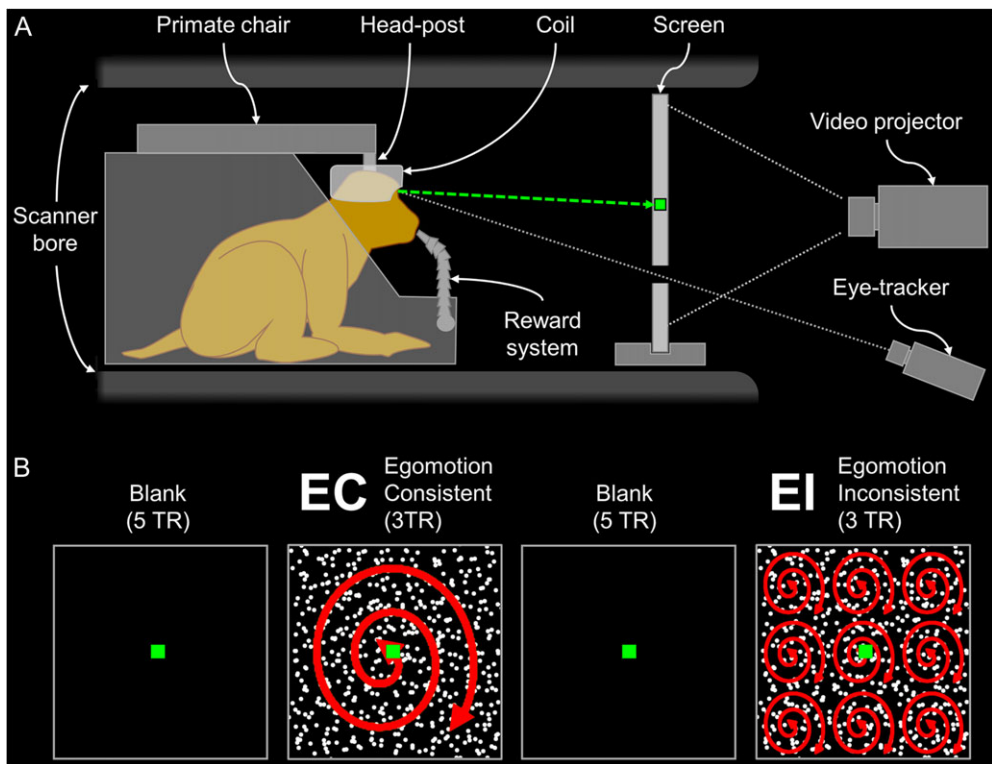


Figure 1. (A) Schematic representation of the monkey fMRI set-up. The animal sits in a sphinx position within the primate chair, in the bore of the scanner, head restrained by the head-post, with the 8 channel, phase array coil located on top of the head. The animal is involved in a passive fixation task, i.e., maintaining the gaze on a green fixation target back-projected on a stimulation screen by a video-projector. Eye position is monitored by an infrared video-based eye-tracker. Correct fixation triggers the delivery of fluid rewards during the runs. (B) Illustration of the stimuli and experimental design. The EC stimulus consisted of a square field of dots moving in a coherent optic flow pattern containing expansion/contraction and rotation components that varied over time, consistent with self-motion on a varying spiral trajectory. The EI stimulus consisted of a 3×3 array of 9 identical panels, each containing a smaller version of the EC stimulus. Recordings were performed using a block-design, with the alternation of EC and EI flow stimuli, separated by blank periods. Each run contained 7 repetitions of such blocks (112 TR in total). EC conditions were shown first in half of the runs and EI conditions appeared first in the other half of the runs.

algorithm (Guizar-Sicairos et al. 2008). This was followed by slice-time correction. A mean image of the functional volumes was then computed for each run and used for normalization on the functional template of the same individual. Those run-dependent normalization parameters were combined to the run-independent parameters linking the functional template to the anatomical one in a single deformation step, during which the functional volumes were resampled at $1 \times 1 \times 1$ mm and slightly smoothed with a spatial Gaussian kernel (FWHM = $1.5 \times 1.5 \times 1.5$ mm).

General Linear Model

Voxel-wise statistics were computed by fitting a general linear model (GLM) to the BOLD signal. The model contained 3 main regressors, representing the 3 experimental conditions: EC, EI, and blank periods (Fig. 1B). Those regressors were convolved with the hemodynamic response function (HRF) estimated from each of the 3 monkeys (HRF estimation from independent data-sets is detailed in Supplementary text 3 and Supplementary Fig. 2). In addition, 4 motion regressors were included in the model. For each run, the slice-by-slice rigid realignment yielded 32 vectors of lateral displacements and 32 vectors of antero-posterior (Y) displacements: One for each slice of the functional volume. The principal component analysis was used to derive 2 lateral and 2 antero-posterior motion regressors, which were entered in the model as nuisance regressors (Vanduffel and Farivar 2014). Both the preprocessing steps and GLM analyses were

implemented in Matlab, with the SPM12 software and custom scripts.

Statistics and Results Presentation

As a first step for identifying potential regions of interest (ROIs) (i.e., regions with consistent BOLD response differences between the EC and EI conditions), the volumetric statistical parametric maps obtained for the EC > EI and EI > EC contrasts in the individual GLM analyses were thresholded at $P < 10^{-3}$ uncorrected (t value > 3.1) and spatially normalized for projection onto the cortical surface of the F99 template. Cortical regions showing significant differences in the same direction between the EC and EI conditions in at least 2 individuals were all considered as ROIs. In a second step, 2 new GLM analyses were performed on each individual after splitting the runs into 2 equal parts (18 runs per GLM, 9 of them with the EC condition first). One GLM was used to look for the presence of individual statistical local maxima in the ROIs or in their immediate vicinity. This search was performed at a relaxed statistical threshold of $P < 10^{-2}$ uncorrected. The GLM performed with the other half of the runs was then used to extract the percent BOLD signal changes (PSC) in cubes of $3 \times 3 \times 3$ voxels centered on the local maxima found with the first GLM. This method avoids the “double dipping” that arises when the same data are used both for identifying ROIs and for measuring activity within them. Small cubes were favored over patches determined by anatomical and/or statistical considerations, because anatomical borders between areas are difficult to

determine precisely and, as we will see below, our contrasts (EC > EI but also EC + EI > baseline) lead to extended activations that cannot be accurately divided into clusters corresponding to different functional regions. Our approach is more conservative and avoids subjectivity when dealing with borders between areas. As we will see in the Results section (cf., the MNI coordinates provided in Table 1), our local maxima are separated enough that we were able to associate a single local maximum with each region and with no overlap between the cubes corresponding to the different regions. Importantly, we assessed that the precise size of those cubes (1, 3 or 5 voxels size) did not have significant impact on the extracted results.

For these cubes, we estimated PSC for the EC and EI conditions relative to the Blank condition as follows:

$$PSC_{EC} = 100 \times (\beta_{EC} - \beta_{Blank}) / \beta_{Constant}$$

$$PSC_{EI} = 100 \times (\beta_{EI} - \beta_{Blank}) / \beta_{Constant}$$

where β_{EC} , β_{EI} , β_{Blank} , and $\beta_{Constant}$ represent the regressor coefficients provided by the GLM analyses. For each region of interest, PSC_{EC} and PSC_{EI} were computed for each run independently, and thus expressed as mean \pm standard error across the runs included in the second GLM (18 runs per monkey). Only regions where PSCs were significantly stronger for the EC than for the EI condition (*t*-tests with $P < 0.05$ and a confidence interval for the difference distribution that does not include 0) were considered for further analysis. Given our number of animals ($n = 3$), there is no statistical test of generalizability. We therefore present the

data on each individual and focus on regions that were consistently found in all the macaques (in at least one hemisphere). In these regions, specificity of the BOLD responses to EC versus EI conditions was quantified by computing a sensitivity ratio of the mean PSC_{EC} and PSC_{EI} with the following formula:

$$\text{Sensitivity ratio (\%)} = 100 \times (PSC_{EC} - PSC_{EI}) / PSC_{EC}.$$

Results

Cortical Network Involved in Processing Optic Flow

In the present study, monkey fMRI techniques are used to characterize the cortical network involved in processing optic flow signals generated by self-motion in nonhuman primate. To that end, 3 macaque monkeys were exposed to optic flow stimuli (moving random dots pattern) either consistent or inconsistent with egomotion (EC and EI conditions, respectively; see Materials and Methods). The experimental design is similar to that developed by Smith et al. in their human fMRI studies (Wall and Smith 2008; Cardin and Smith 2010), allowing a direct comparison of the cortical networks processing optic flow in the 2 primate species (Orban 2002; Orban et al. 2004).

We first assessed the changes in BOLD signal evoked by the visual conditions (EC and EI) relative to baseline (blank screen with fixation point only). These flow stimuli were found to elicit strong statistical increases in BOLD signal across most of the visual cortex in all 3 monkeys (Supplementary Fig. 3A), with a very high degree of overlap between individuals (Supplementary Fig. 3B).

Table 1. Cortical areas activated in at least 3 animals

ROI	M01			M02			M03			Average		
	x	y	z	x	y	z	x	y	z	x	y	z
MSTd												
L	-18	-2	27	-14	-6	29	-13	-4	24	-15	-4	27
R	16	-1	26	14	-4	29	14	-4	26	15	-3	27
FEFsem												
L	-14	23	27	-15	24	29	-15	26	27	-15	24	28
R	13	23	26	12	25	28	-	-	-	13	24	27
VPS												
L	-17	1	28	-19	-3	29	-15	2	27	-17	1	28
R	17	3	27	20	-2	30	-	-	-	19	1	29
7a												
L	-14	-4	30	-15	-7	32	-15	-6	30	-15	-6	31
R	-	-	-	12	-7	34	17	-5	31	15	-6	33
STPm												
L	-	-	-	-20	1	17	-17	2	17	-19	2	17
R	17	2	18	20	0	18	17	1	20	18	1	19
VIP												
L	-8	3	24	-13	3	29	-11	1	27	-11	2	27
R	13	7	27	13	3	29	9	1	24	12	4	27
LIPd												
L	-	-	-	-15	1	33	-15	1	32	-15	1	33
R	-	-	-	14	2	32	16	2	31	15	2	32
FEFsac												
L	-13	23	22	-19	28	21	-15	27	20	-16	26	21
R	-	-	-	17	25	20	-	-	-	17	25	20
pmCSv												
L	-4	15	28	-3	13	27	-3	15	27	-4	14	27
R	-	-	-	2	16	28	-	-	-	2	16	28

Note: Coordinates in MNI space (mm) are those of the statistical local maxima in the left (L) and right (R) hemispheres. Local maxima were determined from the first half of the data and significant selectivity for the EC condition were evaluated from the second half (see details in the text).

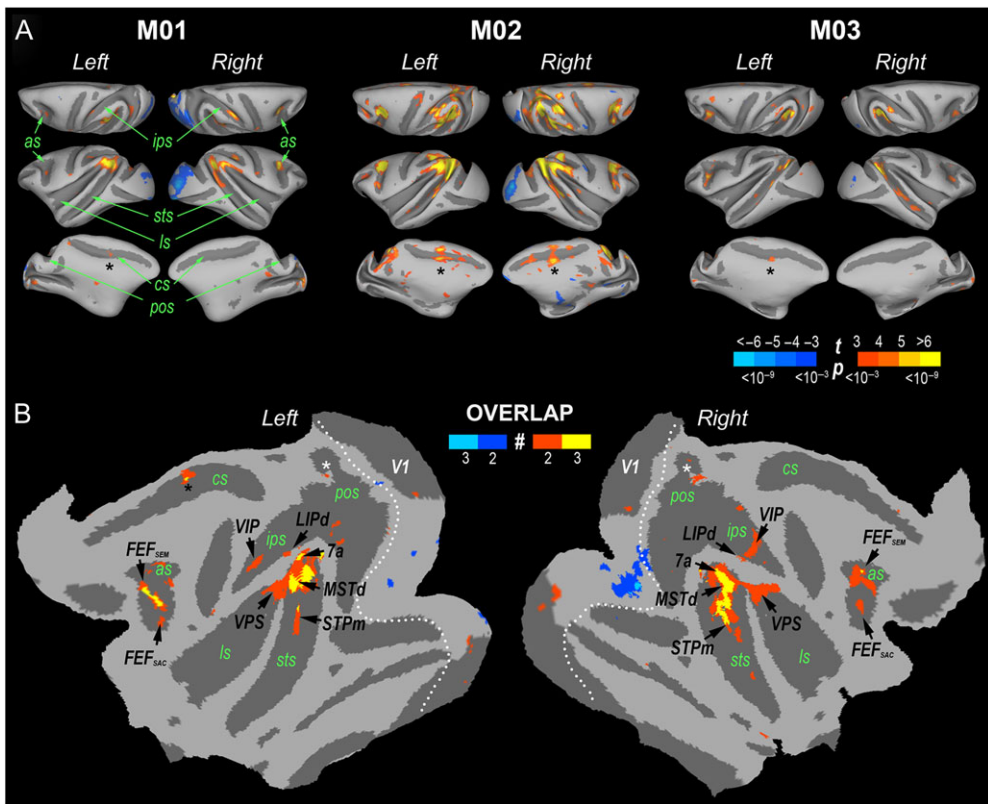


Figure 2. (A) Statistical parametric maps for the EC versus EI contrast in monkeys M01, M02, and M03. Results are projected on dorsal, lateral, and medial views of the left and right hemispheres of the individual cortices. The color code reflects the contrast t-values and indicates statistically significant differences between BOLD responses evoked by the EC and EI conditions ($P < 10^{-3}$ uncorrected). Hot (orange to yellow) and cold (dark to pale blue) colors indicate stronger responses to EC and EI, respectively. (B) Map of overlap between significant activations in the EC versus EI contrast across the 3 monkeys. Only activation sites found in at least 2 individuals are shown. Results are projected on the flattened representations of the left and right hemispheres of the F99 template. Orange and yellow indicate cortical sites significantly more activated by EC than by EI in 2/3 and 3/3 of the subjects, respectively. Dark and pale blue show regions more activated by EI than by EC in 2/3 and 3/3 of the subjects, respectively. Seven cortical areas were significantly activated in our 3 macaques: MSTd, 7a, STPm, VIP, VPS, FEF_{SEM}, and FEF_{SAC}. Black stars indicate a region of the cingulate sulcus (pmCSv) that was found in the 3 animals in the left hemisphere and in one animal on the right hemisphere. White stars indicate a region of the parieto-occipital sulcus where significant activations were found in 2 animals. Borders of the primary visual area (V1) are shown as white dotted lines (as, arcuate sulcus; cs, cingulate sulcus; ips, intraparietal sulcus; ls, lateral sulcus; sts, superior temporal sulcus).

This first analysis indicates that studying the more specific contrast between the EC and EI conditions is not hampered by a lack of statistical power in any of the individuals. Figure 2A shows the statistical parametric maps (t-values) based on all the available data (36 runs/animal) for the EC versus EI contrast in monkeys M01, M02, and M03, projected on dorsal, lateral, and medial views of the individuals left and right cortical hemispheres (see Materials and Methods). Hot colors (orange to yellow) indicate significantly stronger BOLD responses for EC than for EI condition ($P < 10^{-3}$ uncorrected), while cold colors (dark to pale blue) signal the opposite. Despite differences in the extent of the activation patterns observed in the 3 animals (e.g., monkey M02 is generally more responsive than monkeys M01 and M03), preference for the consistent flow (EC > EI) defines a cortical network encompassing the occipital, parietal, temporal, and frontal lobes in all the monkeys. Many nodes of this network are found consistently across the 3 individuals, as revealed in Figure 2B by overlapping the activations observed in at least 2 of the 3 individuals after normalization on the F99 template (Van Essen 2002). Regions color-coded in orange and yellow are those in which EC evokes significantly stronger activations than EI in 2/3 and 3/3 of the monkeys, respectively. Regions with stronger activations for the EI condition are color-coded in dark and pale blue, depending on whether they are found in 2 or 3 animals.

For each of the anatomical regions showing activation overlap, we looked for the presence of statistical local maxima in the native space of each individual. This search was performed on the volumetric statistical parametric maps obtained with GLMs including only half of the runs (18 runs/animal), at a relaxed threshold of $P < 10^{-2}$ uncorrected (see the “Materials and Methods” section). We chose a relaxed threshold in order to avoid the risk of false negatives while using only half of the full dataset. However, the robustness of those activation sites was tested by running paired t-tests on the BOLD signal change profiles obtained at the same sites in the EC and EI conditions in the other half of the runs.

In the following, we describe the activation sites that were identified with the above method in at least one hemisphere in each of the 3 individuals. Two cortical activation sites were found to prefer EC flow in both hemispheres of all our macaques. The most significant one according to the EC versus EI contrast (i.e., global statistical maximum in all 6 hemispheres) was located in the dorso-caudal portion of the superior temporal sulcus (sts), a location corresponding to the dorsal Medial Superior Temporal (MSTd) area. The second site, located within the intraparietal sulcus (ips), matches the location of the VIP. Both MSTd and VIP areas have been repeatedly shown to play a central role in optic flow processing. Note that for VIP, the

activation found in M03 did not overlap those found in M01 and M02, although the local maxima were very close between the 3 animals (see Table 1).

Four other sites were observed in 5 out of 6 hemispheres. One of them was found in the caudal portion of the lateral sulcus (ls), in a location matching that of the VPS (Chen et al. 2011b). Another site was located dorsally in the arcuate sulcus (as), in a portion of the Frontal Eye Field involved in smooth pursuit eye movements (FEFsem) and also recently shown to house neurons responsive to optic flow stimuli (Gu et al. 2015). The third site, in the postero-ventral portion of the inferior parietal lobule, slightly above MSTd, seems to correspond to posterior area 7a, a region that is known to contain neurons that respond to optic flow (e.g., Siegel and Read 1997). Finally, the fourth site lay in the fundus of the sts, anterior to MSTd. This could be part of the superior temporal polysensory area (STP), which also contains motion-sensitive cells with large receptive fields (e.g., Bruce et al. 1981), although STP occupies primarily the upper bank of the sulcus. We tentatively refer to it as STPm after Nelissen et al. (2006) who report motion-sensitive activity at a similar location with fMRI.

Two further sites were found in all 3 individuals, but less reliably across hemispheres (in 4 out of 6 hemispheres). One of them was located in the as, slightly more anterior and lateral than FEFsem, in a location described as a portion of the Frontal Eye Field involved in saccadic eye movements (FEFsac; Gu et al. 2015). Finally, consistent activations were observed within the postero-ventral lip of the cingulate sulcus (black asterisks in Fig. 2A and B), in a region which had not been documented previously as being involved in optic flow processing in monkeys. However, the location of this region echoes that of the recently discovered CSV area in human, which has been shown to be highly selective for the egomotion-compatible optic flow stimuli used in the present study (Wall and Smith 2008; Cardin and Smith 2010). For that reason, we will refer to this cingulate activation site as putative macaque homologue of CSV (pmCSV; see Fig. 2B). Overlapping activations and corresponding local maxima were also identified in 2 out of 3 animals along the dorsal lip of the intraparietal sulcus (LIPd) and within the parieto-occipital sulcus (white asterisks in Fig. 2B). However, only the LIPd maxima were associated with significant differences between the BOLD signals evoked by the EC and EI conditions in both animals. MNI coordinates of the statistical local maxima for the different areas described above are provided in Table 1.

Note that we also found consistent responses for the EI > EC contrast, but they remained largely restricted to the early visual cortex (see blue patches in Fig. 2B). These activations are not caused by local motion characteristics since they are well matched between the 2 conditions. They might be due to the detection of kinetic boundaries (Reppas et al. 1997).

Quantitative Analysis of Egomotion Selectivity

In the following, we characterize in more detail the BOLD response profiles in the cortical regions enumerated above. For each region, the statistical local maximum was localized based on the GLMs performed in half of the runs for each monkey. The response profiles were estimated with the GLMs performed on the other half of the runs (see Materials and Methods). These response profiles correspond to the average responses within cubes of 27 ($3 \times 3 \times 3$) voxels centered on the local maxima localized on the first GLMs. Figures 3 and 4 show the percentage of BOLD signal changes evoked by the EC and EI conditions with respect to the Blank condition within the

8 areas that were activated in all 3 individuals (areas MSTd, VIP, VPS, FEFsem, 7a, STPm, FEFsac, and pmCSV). Voxel-wise statistical parametric maps obtained for the EC > EI contrast in each individual, superimposed on horizontal sections of the individual anatomical templates, are shown in Figs 3A (areas MSTd, VPS, VIP, pmCSV, and FEFsem), 4A (area 7a), and 4C (areas STPm and FEFsac). Their corresponding BOLD profiles are presented in Figs 3B, 4B and D. The asterisks above the profiles indicate statistically significant differences (paired t-test, $P < 10^{-2}$) between the BOLD responses evoked by the EC (white bars) and EI (gray bars) conditions. The percentages of BOLD signal change in area LIPd are shown in Supplementary Fig. 4 for the 2 animals (M02 and M03) that had significantly stronger responses for the EC than for the EI condition in this area.

In order to characterize the strengths of the BOLD responses elicited by the EC stimulus relative to those evoked by the EI stimulus, we computed a sensitivity ratio (in percentage) between the percentages of signal change obtained for these 2 conditions relative to baseline (see the “Materials and Methods” section). These ratios are shown in Fig. 5A for all the 8 areas reported above and their respective locations are illustrated on the cortical surface of the F99 template in Fig. 5B (the positions of these ROIs on the individual cortical surfaces are provided in Supplementary Fig. 5A). In Fig. 5A, the areas are ranked from the highest to the lowest specificity for the EC condition.

This analysis reveals that 2 regions, pmCSV and VPS, emerge as being clearly the most specific for flow stimuli compatible with egomotion, with a near absence of BOLD responses evoked by the egomotion-incompatible stimuli (see also Fig. 3B). In both regions, the mean ratio (across the 3 animals) was above 70% (77% in pmCSV and 70% in VPS), revealing a nearly 4 times larger response for the egomotion-compatible stimuli. Ratios were much lower but still impressive in areas VIP (43%), FEFsac (43%), and FEFsem (39%), and lower still in MSTd (29%), 7a (21%), and STPm (15%). In LIPd (not shown because it was found in only 2 of the 3 individuals), we observed an intermediate ratio of 47%. Note that these sensitivity ratios are robust to changes in the size of the cubes used to define the ROIs (see Supplementary Fig. 5B).

Finally, we estimated differential sensitivity to egomotion-compatible flow within a number of pre-defined visual ROIs taken from the Caret atlas. This enabled us to cross-check our results for regions such as MSTd and also to check that in visual regions such as V1-V3 and MT, where specificity is not expected, it is not seen. The procedure is described in Supplementary text 4. The results, shown in Supplementary Fig. 6, confirmed that selectivity for EC stimuli is seen in MSTd but not in MT, FST (Fundus of the Superior Temporal sulcus), or V4t and was not seen in V1-V3 or V3A. V6 showed weak selectivity (see Discussion).

Discussion

The aim of present study was to identify, in nonhuman primates, the cortical areas involved in processing visual motion produced by self-displacements, i.e., EC optic flow. To that end, we recorded whole-brain BOLD responses from 3 behaving macaques while they were exposed to optic flow stimuli either consistent or inconsistent with egomotion (Fig. 1). The visual stimuli and experimental design were similar to those used in previous human fMRI studies (Wall and Smith 2008; Cardin and Smith 2010), allowing a direct comparison of the cortical networks between human and nonhuman primates. Our results reveal that in macaque, as in human, many cortical areas are more strongly activated by EC optic flow stimuli. Those regions are broadly

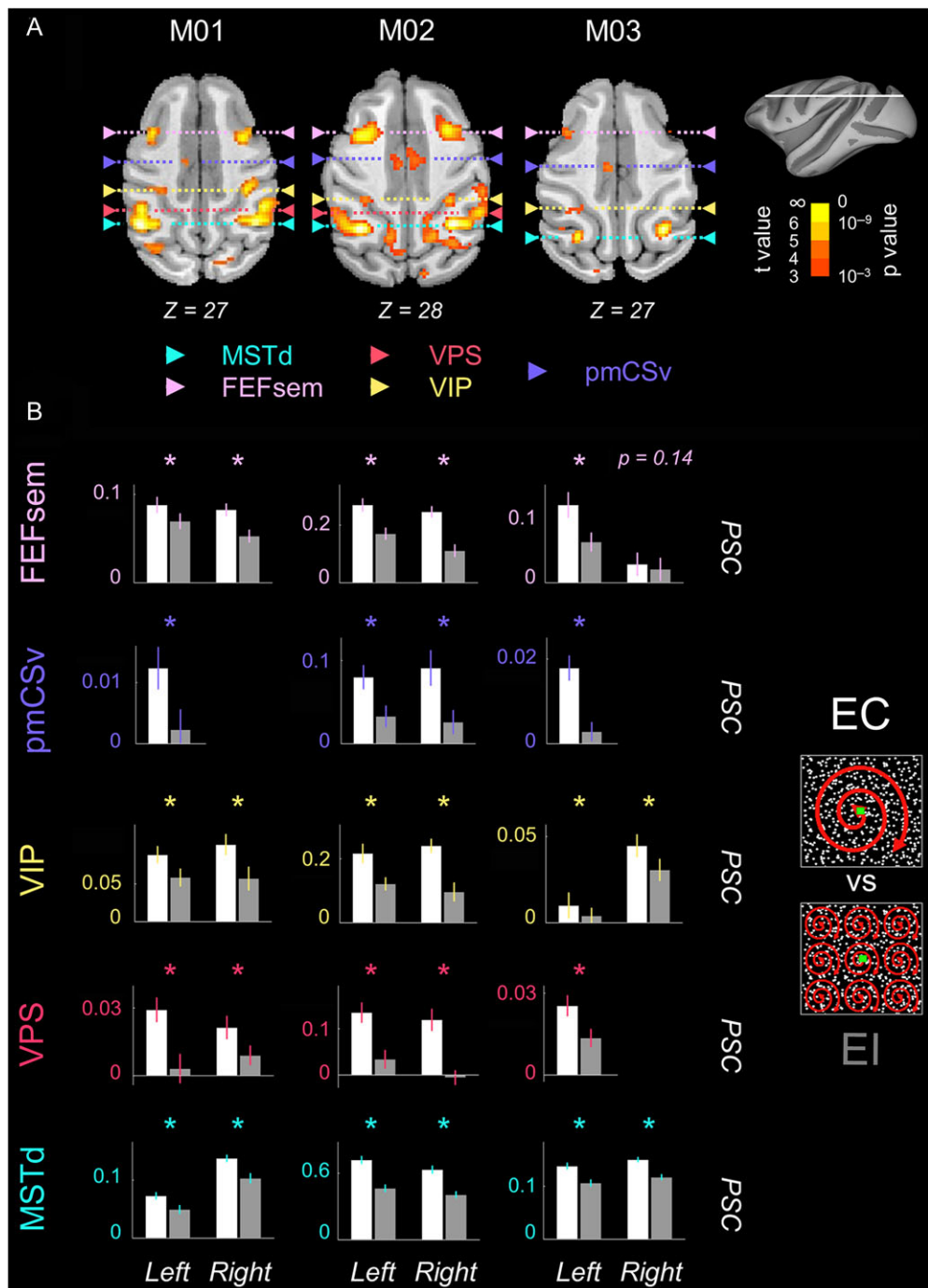


Figure 3. Activity profiles in areas MSTd, VPS, VIP, pmCSv, and FEFsem. (A) Statistical results of the EC > EI contrast shown on axial sections for monkeys M01, M02, and M03 (neurological convention). Areas are indicated by arrows on the 3 monkeys. (B) PSC in these 5 areas for the EC and EI conditions with respect to baseline (blank condition) in both hemispheres of the 3 macaques. The first half of the data was used to define ROIs around the local maxima of these areas and the second half was used to compute PSC (see details in the text). The error bars provide the standard errors across runs ($n = 18$). Stars indicate areas whose PSCs during the EC condition were significantly stronger than during the EI condition (t-tests, $P < 0.05$). P-values of the t-tests are provided for areas that did not pass significance.

distributed, encompassing the temporal, parietal, frontal, and cingulate cortices (Fig. 2). They are now discussed in more detail.

Activations in Temporal Cortex: MSTd and STPm

In all 6 recorded hemispheres, the most statistically significant activations for the contrast between EC and EI stimuli was found in a dorso-caudal portion of the sts, which corresponds

in macaque to area MSTd (Fig. 3). In order to check that these activations were well localized in MSTd and did not overlap with adjacent areas like MT, FST, or V4t, we performed an additional analysis from anatomical atlases provided in the Caret software (see Supplementary text 4 and Supplementary Fig. 6). This analysis confirmed that our activations are specific to MSTd. Numerous electrophysiological studies have shown that MSTd houses neurons selective to optic flow stimuli presented

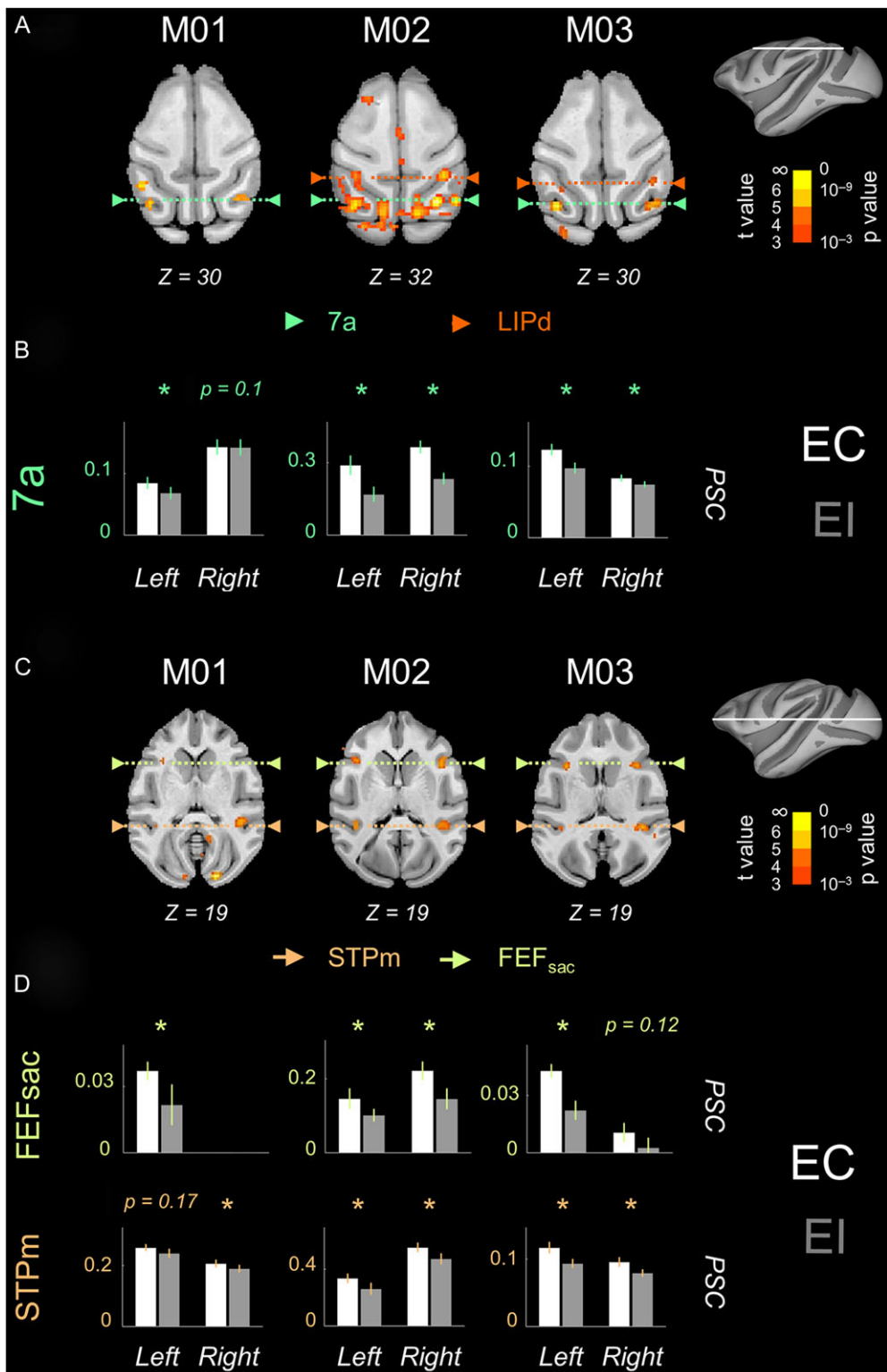


Figure 4. Activity profiles in areas 7a, FEF_{sac}, and STPm. (A) Statistical results of the EC > EI contrast shown on axial sections for the 3 monkeys. Areas 7a (in all monkeys) and LIPd (in M02 and M03) are indicated by arrows. (B) PSC in area 7a for the EC and EI conditions with respect to baseline. (C) Statistical results of the EC > EI contrast shown on axial sections for the 3 monkeys. Areas STPm and FEF_{sac} are indicated by arrows. (D) PSC in areas FEF_{sac} and STPm for the EC and EI conditions with respect to baseline. Other details as in Fig. 3.

in their receptive fields (e.g., Tanaka et al. 1989; Duffy and Wurtz 1991), as well as to inertial vestibular stimulation (e.g., Duffy 1998; Takahashi et al. 2007). Moreover, both

microstimulation and reversible inactivation indicate a causal role for MSTd in heading perception (Britten and van Wezel 2002; Gu et al. 2012). Together, these characteristics point to a

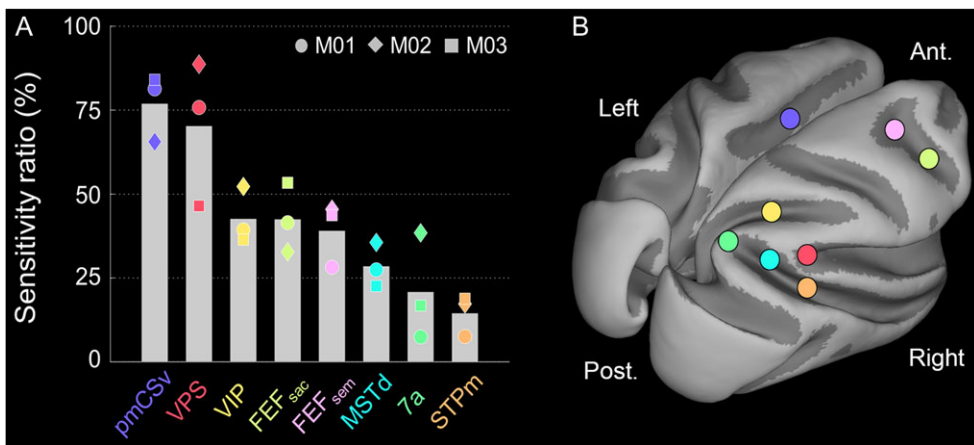


Figure 5. (A) Average sensitivity ratio (%) between the responses to the EC and EI conditions. The ratio (defined in the text) may be thought of as the reduction in response that occurs when an EC stimulus is replaced with EI. As for the PSC, ratios were computed on the second half of the data (see details in the text). Only areas with significant responses in the 3 animals are shown. Areas were sorted according to their mean sensitivity ratio. Markers provide the individual data corresponding to M01 (circles), M02 (diamonds), and M03 (squares). (B) Schematic localization of the 8 areas on the F99 template.

central role for MSTd in processing visual motion produced by self-displacements. Our data also revealed that the sensitivity ratio between responses to consistent and inconsistent flow stimuli is not very high (29%; see Fig. 5), suggesting that flow stimuli that are not consistent with self-displacements can nevertheless evoke strong responses in MSTd neurons. Interestingly, our results are in broad agreement with those obtained in hMST using the same experimental protocol (Wall and Smith 2008). These authors reported about 15% reduction in response to incompatible flow in hMST, compared with about 30% found here in macaque MSTd. This difference is consistent and could reflect a species difference, suggesting a greater specialization in macaque than human. However, it should be remembered that hMST in humans, which is defined simply in terms of the presence of strong ipsilateral drive (absent in hMT), probably does not correspond exactly to MSTd and may include other motion-sensitive regions with large receptive fields. It is therefore unsafe to make a direct comparison of results. Our results leave open the possibility that hMST, or some part of it, is homologous with MSTd for optic flow processing.

Another temporal activation site was observed in all the animals (5/6 hemispheres), situated more anteriorly along the fundus and the dorsal lip of the sts. This site may correspond to a subregion of the STP area, in which neurons selective to optic flow stimuli have been reported (Bruce et al. 1981; Anderson and Siegel 1999), although neurophysiological studies describe STP as located in the upper bank and fundus of sts whereas our cases show activity mainly in the lower bank (Fig. 2A), albeit with overlap across animals mainly in the fundus (Fig. 2B). In a recent monkey fMRI study, Nelissen et al. (2006) confirmed the existence of an optic-flow sensitive region in STP, that they named STPm and whose location is close to that found in the present study (Fig. 4), although again STPm is mainly in the upper bank of the sulcus. Interestingly, Nelissen et al. noted that responses to optic flow stimuli in STPm are similar to those of MSTd, except that the amplitude is lower. This difference is also found in the present study, together with a slightly lower sensitivity ratio (15%) of STPm. In human, a region within the sts and anterior to the hMT+ complex has been recently proposed as a putative homologue of macaque STP (Beauchamp et al. 2004b; Smith et al. 2012). This region was named STSms (STS multi-sensory) because of its multi-sensory

responses (Beauchamp et al. 2004a, 2004b, 2008). Among other modalities, STSms is activated by visual (Beauchamp et al. 2004b) and vestibular (Smith et al. 2012) signals. Therefore, it might be involved in the processing of EC optic flow. However, STSms was not significantly activated by our contrast in 2 human studies based on the same experimental protocol (Wall and Smith 2008; Cardin and Smith 2010). How can this be explained? One possibility might be simply that differential activity was missed in human STSms because of sensitivity limitations (e.g., the human studies used considerably fewer stimulus repetitions). Another is that STSms is not in fact homologous with STPm, or is broadly homologous but differs in its degree of specialization. Further investigations will be needed to clarify this point.

Activations in Parietal Cortex: VIP, 7a, and LIPd

In our 3 animals (6/6 hemispheres), we found statistically significant activation for the EC versus EI contrast in the fundus of the ips, which houses area VIP in macaque (Fig. 3). Together with MSTd, VIP is generally considered as playing a central role in processing heading information provided by both visual and vestibular signals (Bremmer et al. 2002a, 2002b). VIP and MSTd neurons seem to share many characteristics in the way they code both visual and inertial movements (Schaafsma and Duysens 1996; Chen et al. 2011a). However, the mean sensitivity ratio we measured in VIP (43%) was greater than that found in MSTd (Fig. 5). In human, the same contrast significantly activates a region within the anterior part of the ips (see e.g., Wall and Smith 2008) whose coordinates are very close to those of the polysensory motion sensitive area originally described by Bremmer et al. (2001) and proposed as a putative homologue of macaque VIP (hVIP). Wall and Smith (2008) reported a 46% response reduction for EI stimuli, very similar to our result for macaque VIP. Our data are therefore consistent with the hypothesis of a correspondence between these 2 areas, although caution is needed because the ips is organized differently in humans and macaques, with several more areas in humans.

Besides VIP, a consistent site of parietal activation, observed in all our monkeys (5/6 hemispheres), was located within area 7a, which occupies an elongated posterior portion of the inferior parietal lobule (Fig. 4). Area 7a is involved in spatial vision,

through the integration of visual and oculomotor signals (Mishkin et al. 1982; Anderson and Siegel 1999). Both electrophysiological and optical imaging studies have shown that 7a neurons respond selectively to optic flow stimuli (Siegel and Read 1997; Phinney and Siegel 2000; Merchant et al. 2001; Raffi and Siegel 2007). More recently, cytoarchitectonic differences along the inferior parietal lobule have led to its subdivision into 4 sectors: PF, PFG, PG, and Opt (Pandya and Seltzer 1982; Gregoriou et al. 2006). The posterior location of our activation site, together with the fact that it extends ventrally into the dorsal bank of the STS, strongly suggest that it corresponds to the caudal-most region Opt (Gregoriou et al. 2006). Interestingly, tracer injections in Opt (Rozzi et al. 2006) revealed strong connections with the temporal areas that we found to be involved in processing egomotion-compatible optic flow: MSTd and STP, and much weaker connections with the neighboring temporal areas MT and FST. The same study revealed that Opt is also connected to LIP in the ips and to area 23, in the cingulate sulcus, 2 sites that also responded more strongly to consistent than inconsistent optic flow stimuli in a majority of recorded hemispheres, as will be discussed below.

The dorsal part of the lateral intraparietal (LIPd) area was the third site of parietal activation evidenced in the present study (see Fig. 3 and Supplementary Fig. 4). Results were less systematic than those of area 7a/Opt, with 4 out of 6 hemispheres, but closely resembled those found in VIP (with an average sensitivity ratio of 47%). To our knowledge, there is no previous study linking LIPd to the specific processing of egomotion-compatible optic flow. However, the present results, together with the fact that LIPd is connected to 7a/Opt, argue that the possible role of LIPd in optic flow processing deserves further investigation.

Several studies have reported the existence of a possible homologue of macaque area LIP in the human superior parietal cortex (Sereno et al. 2001; Shikata et al. 2008). To our knowledge, the human homologue of area 7a has not been firmly established. In any case, the only robust and reliable activations that were found near ips in human using the same protocol corresponded to area hVIP (see above). Our results therefore suggest that processing of optic flow in 7a (and LIPd, if confirmed) may be specific to macaque.

Activation in Parieto-Insular Cortex: VPS

In our 3 individuals (5/6 hemispheres) stronger BOLD responses for the EC optic flow stimuli were observed in the caudal portion of the sylvian fissure (Fig. 3). The location of this activation site corresponds to the VPS area, which is posterior to the PIVC from which it receives vestibular inputs. VPS is also connected to MSTd (Guldin et al. 1992), which may feed VPS with visual optic flow information. In agreement with this view, VPS neurons have been shown to integrate heading-related information from both visual optic-flow and vestibular signals (Chen et al. 2011b). Importantly, our results revealed that after pmCSV, VPS is actually the cortical region exhibiting the greatest sensitivity ratio for EC stimuli (70%, see Fig. 5), much higher than those found in the temporal and parietal activation sites described so far. In human, the same contrast (Cardin and Smith 2010) also revealed a parieto-insular region, PIC (that was originally mistakenly labeled as PIVC), sharing most of the properties described here for VPS and notably its responsiveness to vestibular inputs (Smith et al. 2012). The sensitivity ratio in PIC is very high (~80%; Cardin and Smith 2010) and close to the one

we found in macaque VPS. Altogether, these results further support the idea that these 2 regions are homologous.

Activations in Frontal Cortex: FEFsem and FEFsac

In 3 animals (5/6 hemispheres), strong activations were found in the dorsal part of the as (Fig. 3). This location matches that of FEFsem, a subregion of the frontal eye field involved in the control of smooth pursuit eye movements (Lynch 1987; MacAvoy et al. 1991). The average sensitivity ratio we found in FEFsem (39%) was about the same as those of MSTd, VIP and 7a/Opt, which all share strong recurrent connections with FEFsem (Boussaoud et al. 1990; Maioli et al. 1998; Stanton et al. 2005). Recently, FEFsem neurons have been shown to respond selectively to visual and vestibular signals induced by self-displacements (Gu et al. 2015). Thus, the present results provide further evidence that FEFsem processes heading information.

In 4/6 hemispheres, (3 individuals), a second site of activation was observed within the as. Located slightly more anterior and lateral than FEFsem, within the fundus and anterior branch of the as (Fig. 4), it nicely fits the anatomical location reported for another subregion of the frontal eye field, FEFsac, which is involved in saccadic eye movements (MacAvoy et al. 1991; Gu et al. 2015). Our analyses of eye movements reveal differences neither in the quality of fixation nor in the number of saccades evoked by EC and EI stimuli, in any of the 3 individuals (see Supplementary text 2 and Supplementary Fig. 1). Thus, the present results argue for a secondary role of FEFsac in the processing of visual motion induced by self-displacements.

In human, studies that used the same experimental protocol (Wall and Smith 2008; Cardin and Smith 2010) did not report any significant activation in or around the frontal eye field region. A re-examination of these data revealed that a few subjects (<20%) actually had significant responses in FEF. This low proportion makes it difficult to determine whether these activations were false positive. Either way, this comparison across species supports the idea that the implication of the FEFsem and FEFsac regions in optic flow processing is at least more pronounced in macaque.

Activation in Cingulate Cortex: pmCSV

In human, a growing number of fMRI studies have described a region within the cingulate sulcus, CSv, which is significantly activated by complex motion patterns (Wall and Smith 2008; Fischer et al. 2012; Pitzalis et al. 2013; Schindler and Bartels 2016). Using the stimuli of the present study, Cardin and Smith (2010) reported that this region had the greatest specificity for EC optic flow, in virtually all the tested subjects. In all our animals (4/6 hemispheres), we measured strong responses in the posterior cingulate sulcus (Fig. 3). Atlas-based comparison in Caret software indicates that this activation site belongs to area 23c (Vogt et al. 2005), which is thought to be involved in spatial vision notably through its connection to area 7a/Opt (Vogt et al. 1992; Rozzi et al. 2006). A striking feature of the activity profiles for the 4 significant hemispheres is the near absence of response to EI stimuli (Fig. 3) which leads to a very high sensitivity ratio (77%, see Fig. 5), as has been found in human CSv (Wall and Smith 2008). Although other studies will be needed to confirm the possible homology between pmCSV and CSv, the identification of pmCSV provides new opportunities to understand activations in human CSv by reference to electrophysiological explorations in macaque.

Homologies with the Human EC-Selective Areas V6, Pc, and 2v?

In human, the contrast used in this study leads to consistent activations in the parieto-occipital cortex (Cardin and Smith 2010), in a site that both retinotopic mapping and response properties point to as the human homologue of macaque area V6 (Pitzalis et al. 2006, 2010; Cardin et al. 2012b). In the present study, our voxel-wise analysis did not reveal any evidence that V6 prefers EC optic flow. However, a suggestive trend was observed in the atlas-based approach (see Supplementary text 4 and Supplementary Fig. 6), which shows a sensitivity ratio for V6 of about 20% that is consistent across the 3 animals. This leaves open the possibility that V6 does possess EC selectivity but that this was not reliable enough to be detected at the voxel level. It is also possible that there is no such selectivity and the trend arises from erroneous inclusion of parts of neighboring visual regions, although the immediate neighbors V2, V3, and V3A do not themselves show strong specificity. Whatever the explanation, our results indicate that selectivity to the EC condition in macaque V6 is not as robust as in hV6. One possible interpretation of this discrepancy might be that human and monkey V6 differ regarding their involvement in heading processing, the involvement being greater in humans. More generally, this observation reinforces the view that the cortical processing of visual motion might differ in several aspects between these 2 primate species (Vanduffel et al. 2002; Orban et al. 2003).

Finally, it should be noted that 2 other human cortical regions have been reported to show selective responses to EC stimuli (Cardin and Smith 2010) that do not appear to do so in macaque. The first is a possible homologue of macaque area 2v in anterior parietal cortex, which has been shown to receive vestibular afferents and may therefore process self-motion. The second is an anterior region of the precuneus, termed Pc by these authors. Since little is known about either region, it is difficult to interpret these differences. At least in Pc, and possibly also in putative human 2v, the difference between EC and EI reflects differences in visual suppression rather than visual responses.

Conclusion

Overall, our results are in excellent agreement with the electrophysiological and anatomical data collected over recent decades in macaque monkey. They demonstrate that a simple contrast between optic flow stimuli that are consistent or inconsistent with self-displacements can reveal the vast majority of cortical areas known to be involved in processing heading information through optic flow, including those also thought to integrate vestibular inputs. An advantage of the monkey fMRI approach is that it allows a direct comparison with results obtained in several human studies based on the same contrast (Wall and Smith 2008; Cardin and Smith 2010). Together, the data collected in the 2 species suggest that although the networks processing optic flow in human and macaque share some properties (i.e., possible homologies between areas MST/hMST, VIP/hVIP, VPS/PIC, and pmCSv/CSV), they nonetheless remain different. On the one hand, some of the significantly activated areas in macaque (7a, STPm, FEFsem and also FEFsac) were not found in human. On the other hand, some areas robustly found in humans (V6, P2v, Pc) did not show significant activations in the present study.

Supplementary Material

Supplementary material are available at *Cerebral Cortex* online.

Funding

CNRS, from the ANR (ANR-13-JSV4-0007-01; ANR-12-BSV4-0005); European Council (Marie Curie grant PIIF-GA-2011-298386 Real-Depth).

Notes

The authors thank A. Sadoun for his help during the surgery and the technical personnel of the Cerco monkey facility for their help with the handling of the animals. We also thank the radiographers of the INSERM U214 TONIC MRI platform for their help with the (f)MRI recordings and M. Furlan for help with generating visual stimuli. Conflict of Interest: None declared.

References

- Anderson KC, Siegel RM. 1999. Optic flow selectivity in the anterior superior temporal polysensory area, STPa, of the behaving monkey. *J Neurosci*. 19:2681–2692.
- Antal A, Baudewig J, Paulus W, Dechent P. 2008. The posterior cingulate cortex and planum temporale/parietal operculum are activated by coherent visual motion. *Vis Neurosci*. 25:17–26.
- Beauchamp MS, Argall BD, Bodurka J, Duyu JH, Martin A. 2004a. Unraveling multisensory integration: patchy organization within human STS multisensory cortex. *Nat Neurosci*. 7: 1190–1192.
- Beauchamp MS, Lee KE, Argall BD, Martin A. 2004b. Integration of auditory and visual information about objects in superior temporal sulcus. *Neuron*. 41:809–823.
- Beauchamp MS, Yasar NE, Frye RE, Ro T. 2008. Touch, sound and vision in human superior temporal sulcus. *Neuroimage*. 41:1011–1020.
- Boussaoud D, Ungerleider LG, Desimone R. 1990. Pathways for motion analysis: cortical connections of the medial superior temporal and fundus of the superior temporal visual areas in the macaque. *J Comp Neurol*. 296:462–495.
- Bremmer F, Duhamel J-R, Ben Hamed S, Graf W. 2002a. Heading encoding in the macaque ventral intraparietal area (VIP). *Eur J Neurosci*. 16:1554–1568.
- Bremmer F, Klam F, Duhamel J-R, Ben Hamed S, Graf W. 2002b. Visual-vestibular interactive responses in the macaque ventral intraparietal area (VIP). *Eur J Neurosci*. 16:1569–1586.
- Bremmer F, Schlack A, Shah NJ, Zafiris O, Kubischik M, Hoffmann K-P, Zilles K, Fink GR. 2001. Polymodal motion processing in posterior parietal and premotor cortex: a human fMRI study strongly implies equivalencies between humans and monkeys. *Neuron*. 29:287–296.
- Britten KH, van Wezel RJA. 2002. Area MST and heading perception in macaque monkeys. *Cereb Cortex*. 12:692–701.
- Bruce C, Desimone R, Gross CG. 1981. Visual properties of neurons in a polysensory area in superior temporal sulcus of the macaque. *J Neurophysiol*. 46:369–384.
- Cardin V, Hemsworth L, Smith AT. 2012a. Adaptation to heading direction dissociates the roles of human MST and V6 in the processing of optic flow. *J Neurophysiol*. 108:794–801.
- Cardin V, Sherrington R, Hemsworth L, Smith AT. 2012b. Human V6: functional characterisation and localisation. *PLoS One*. 7:e47685.
- Cardin V, Smith AT. 2010. Sensitivity of human visual and vestibular cortical regions to egomotion-compatible visual stimulation. *Cereb Cortex*. 20:1964–1973.
- Chen A, DeAngelis GC, Angelaki DE. 2011a. Representation of vestibular and visual cues to self-motion in ventral intraparietal cortex. *J Neurosci*. 31:12036–12052.

- Chen A, DeAngelis GC, Angelaki DE. 2011b. Convergence of vestibular and visual self-motion signals in an area of the posterior sylvian fissure. *J Neurosci.* 31:11617–11627.
- Chen A, Gu Y, Liu S, DeAngelis GC, Angelaki DE. 2016. Evidence for a causal contribution of macaque vestibular, but not intraparietal, cortex to heading perception. *J Neurosci.* 36: 3789–3798.
- Duffy CJ. 1998. MST neurons respond to optic flow and translational movement. *J Neurophysiol.* 80:1816–1827.
- Duffy CJ, Wurtz RH. 1991. Sensitivity of MST neurons to optic flow stimuli. I. A continuum of response selectivity to large-field stimuli. *J Neurophysiol.* 65:1329–1345.
- Duffy CJ, Wurtz RH. 1995. Response of monkey MST neurons to optic flow stimuli with shifted centers of motion. *J Neurosci.* 15:5192–5208.
- Duffy FH, Burchfiel JL, Conway JL. 1976. Bicuculline reversal of deprivation amblyopia in the cat. *Nature.* 260:256–257.
- Dukelow SP, DeSouza JF, Culham JC, van den Berg AV, Menon RS, Vilis T. 2001. Distinguishing subregions of the human MT+ complex using visual fields and pursuit eye movements. *J Neurophysiol.* 86:1991–2000.
- Fan RH, Liu S, DeAngelis GC, Angelaki DE. 2015. Heading tuning in Macaque Area V6. *J Neurosci.* 35:16303–16314.
- Fetsch CR, Pouget A, DeAngelis GC, Angelaki DE. 2012. Neural correlates of reliability-based cue weighting during multi-sensory integration. *Nat Neurosci.* 15:146–154.
- Fischer E, Bülthoff HH, Logothetis NK, Bartels A. 2012. Visual motion responses in the posterior cingulate sulcus: a comparison to V5/MT and MST. *Cereb Cortex.* 22:865–876.
- Frank SM, Baumann O, Mattingley JB, Greenlee MW. 2014. Vestibular and visual responses in human posterior insular cortex. *J Neurophysiol.* 112:2481–2491.
- Galletti C, Gamberini M, Kutz DF, Fattori P, Luppino G, Matelli M. 2001. The cortical connections of area V6: an occipito-parietal network processing visual information. *Eur J Neurosci.* 13:1572–1588.
- Gregoriou GG, Borra E, Matelli M, Luppino G. 2006. Architectonic organization of the inferior parietal convexity of the macaque monkey. *J Comp Neurol.* 496:422–451.
- Grossberg S, Mingolla E, Pack C. 1999. A neural model of motion processing and visual navigation by cortical area MST. *Cereb Cortex.* 9:878–895.
- Gu Y, Cheng Z, Yang L, DeAngelis GC, Angelaki DE. 2015. Multisensory convergence of visual and vestibular heading cues in the pursuit area of the frontal eye field. *Cereb Cortex.* 26:3785–3801.
- Gu Y, DeAngelis GC, Angelaki DE. 2012. Causal links between dorsal medial superior temporal area neurons and multi-sensory heading perception. *J Neurosci.* 32:2299–2313.
- Gu Y, Watkins PV, Angelaki DE, DeAngelis GC. 2006. Visual and nonvisual contributions to three-dimensional heading selectivity in the medial superior temporal area. *J Neurosci.* 26:73–85.
- Guizar-Sicairos M, Thurman ST, Fienup JR. 2008. Efficient sub-pixel image registration algorithms. *Opt Lett.* 33:156–158.
- Guldin WO, Akbarian S, Grüsser O-J. 1992. Cortico-cortical connections and cytoarchitectonics of the primate vestibular cortex: a study in squirrel monkeys (*Saimiri sciureus*). *J Comp Neurol.* 326:375–401.
- Huk AC, Dougherty RF, Heeger DJ. 2002. Retinotopy and functional subdivision of human areas MT and MST. *J Neurosci.* 22:7195–7205.
- Kolster H, Peeters R, Orban GA. 2010. The retinotopic organization of the human middle temporal area MT/V5 and its cortical neighbors. *J Neurosci.* 30:9801–9820.
- Komatsu H, Wurtz RH. 1988. Relation of cortical areas MT and MST to pursuit eye movements. I. Localization and visual properties of neurons. *J Neurophysiol.* 60:580–603.
- Lynch JC. 1987. Frontal eye field lesions in monkeys disrupt visual pursuit. *Exp Brain Res.* 68:437–441.
- MacAvoy MG, Gottlieb JP, Bruce CJ. 1991. Smooth-pursuit eye movement representation in the primate frontal eye field. *Cereb Cortex.* 1:95–102.
- Maioli MG, Squatrito S, Samolsky-Dekel BG, Riva Sanseverino E. 1998. Corticocortical connections between frontal periarcuate regions and visual areas of the superior temporal sulcus and the adjoining inferior parietal lobule in the macaque monkey. *Brain Res.* 789:118–125.
- McLaren DG, Kosmatka KJ, Kastman EK, Bendlin BB, Johnson SC. 2010. Rhesus macaque brain morphometry: a methodological comparison of voxel-wise approaches. *Methods.* 50: 157–165.
- McLaren DG, Kosmatka KJ, Oakes TR, Kroenke CD, Kohama SG, Matochik JA, Ingram DK, Johnson SC. 2009. A population-average MRI-based atlas collection of the rhesus macaque. *Neuroimage.* 45:52–59.
- Mendoza-Halliday D, Torres S, Martinez-Trujillo JC. 2014. Sharp emergence of feature-selective sustained activity along the dorsal visual pathway. *Nat Neurosci.* 17:1255–1262.
- Merchant H, Battaglia-Mayer A, Georgopoulos AP. 2001. Effects of optic flow in motor cortex and area 7a. *J Neurophysiol.* 86: 1937–1954.
- Mineault PJ, Khawaja FA, Butts DA, Pack CC. 2012. Hierarchical processing of complex motion along the primate dorsal visual pathway. *Proc Natl Acad Sci USA.* 109:E972–E980.
- Mishkin M, Lewis ME, Ungerleider LG. 1982. Equivalence of parieto-preoccipital subareas for visuospatial ability in monkeys. *Behav Brain Res.* 6:41–55.
- Morrone MC, Tosetti M, Montanaro D, Fiorentini A, Cioni G, Burr DC. 2000. A cortical area that responds specifically to optic flow, revealed by fMRI. *Nat Neurosci.* 3:1322–1328.
- Motter BC, Mountcastle VB. 1981. The functional properties of the light-sensitive neurons of the posterior parietal cortex studied in waking monkeys: foveal sparing and opponent vector organization. *J Neurosci.* 1:3–26.
- Nelissen K, Vanduffel W, Orban GA. 2006. Charting the lower superior temporal region, a new motion-sensitive region in monkey superior temporal sulcus. *J Neurosci.* 26:5929–5947.
- Orban GA. 2002. Functional MRI in the awake monkey: the missing link. *J Cogn Neurosci.* 14:965–969.
- Orban GA, Fize D, Peuskens H, Denys K, Nelissen K, Sunaert S, Todd J, Vanduffel W. 2003. Similarities and differences in motion processing between the human and macaque brain: evidence from fMRI. *Neuropsychologia.* 41:1757–1768.
- Orban GA, Van Essen D, Vanduffel W. 2004. Comparative mapping of higher visual areas in monkeys and humans. *Trends Cogn Sci.* 8:315–324.
- Pandya DN, Seltzer B. 1982. Intrinsic connections and architectonics of posterior parietal cortex in the rhesus monkey. *J Comp Neurol.* 204:196–210.
- Perrone JA, Stone LS. 1994. A model of self-motion estimation within primate extrastriate visual cortex. *Vision Res.* 34: 2917–2938.
- Phinney RE, Siegel RM. 2000. Speed selectivity for optic flow in area 7a of the behaving macaque. *Cereb Cortex.* 10: 413–421.
- Pitzalis S, Galletti C, Huang R-S, Patria F, Committeri G, Galati G, Fattori P, Sereno MI. 2006. Wide-field retinotopy defines human cortical visual area V6. *J Neurosci.* 26:7962–7973.

- Pitzalis S, Sdoia S, Bultrini A, Committeri G, Di Russo F, Fattori P, Galletti C, Galati G. 2013. Selectivity to translational egomotion in human brain motion areas. *PLoS One.* 8:e60241.
- Pitzalis S, Sereno MI, Committeri G, Fattori P, Galati G, Patria F, Galletti C. 2010. Human v6: the medial motion area. *Cereb Cortex.* 20:411–424.
- Raffi M, Siegel RM. 2007. A functional architecture of optic flow in the inferior parietal lobule of the behaving monkey. *PLoS One.* 2:e200.
- Reppas JB, Niyogi S, Dale AM, Sereno MI, Tootell RB. 1997. Representation of motion boundaries in retinotopic human visual cortical areas. *Nature.* 388:175–179.
- Rozzi S, Calzavara R, Belmalih A, Borrà E, Gregoriou GG, Matelli M, Luppino G. 2006. Cortical connections of the inferior parietal cortical convexity of the macaque monkey. *Cereb Cortex.* 16: 1389–1417.
- Schaafsma SJ, Duysens J. 1996. Neurons in the ventral intraparietal area of awake macaque monkey closely resemble neurons in the dorsal part of the medial superior temporal area in their responses to optic flow patterns. *J Neurophysiol.* 76:4056–4068.
- Schindler A, Bartels A. 2016. Connectivity reveals sources of predictive coding signals in early visual cortex during processing of visual optic flow. *Cereb Cortex.* pii:bhw136 [Epub ahead of print].
- Sereno MI, Pitzalis S, Martinez A. 2001. Mapping of contralateral space in retinotopic coordinates by a parietal cortical area in humans. *Science.* 294:1350–1354.
- Shikata E, McNamara A, Sprenger A, Hamzei F, Glauche V, Büchel C, Binkofski F. 2008. Localization of human intraparietal areas AIP, CIP, and LIP using surface orientation and saccadic eye movement tasks. *Hum Brain Mapp.* 29: 411–421.
- Siegel RM, Read HL. 1997. Analysis of optic flow in the monkey parietal area 7a. *Cereb Cortex.* 7:327–346.
- Smith AT, Wall MB, Thilo KV. 2012. Vestibular inputs to human motion-sensitive visual cortex. *Cereb Cortex.* 22:1068–1077.
- Smith AT, Wall MB, Williams AL, Singh KD. 2006. Sensitivity to optic flow in human cortical areas MT and MST. *Eur J Neurosci.* 23:561–569.
- Stanton GB, Friedman HR, Dias EC, Bruce CJ. 2005. Cortical afferents to the smooth-pursuit region of the macaque monkey's frontal eye field. *Exp Brain Res.* 165:179–192.
- Steinmetz MA, Motter BC, Duffy CJ, Mountcastle VB. 1987. Functional properties of parietal visual neurons: radial organization of directionalities within the visual field. *J Neurosci.* 7:177–191.
- Takahashi K, Gu Y, May PJ, Newlands SD, DeAngelis GC, Angelaki DE. 2007. Multimodal coding of three-dimensional rotation and translation in area MSTd: comparison of visual and vestibular selectivity. *J Neurosci.* 27:9742–9756.
- Tanaka K, Fukada Y, Saito HA. 1989. Underlying mechanisms of the response specificity of expansion/contraction and rotation cells in the dorsal part of the medial superior temporal area of the macaque monkey. *J Neurophysiol.* 62: 642–656.
- Van Essen DC. 2002. Surface-based atlases of cerebellar cortex in the human, macaque, and mouse. *Ann NY Acad Sci USA.* 978:468–479.
- Van Essen DC, Drury HA, Dickson J, Harwell J, Hanlon D, Anderson CH. 2001. An integrated software suite for surface-based analyses of cerebral cortex. *J Am Med Inform Assoc.* 8:443–459.
- Vanduffel W, Farivar R. 2014. Functional MRI of awake behaving macaques using standard equipment. In: Duric D, editor. *Advanced Brain Neuroimaging Topics in Health and Disease – Methods and Applications.* InTech, DOI: 10.5772/58281. Available from: <http://www.intechopen.com/books/advanced-brain-neuroimaging-topics-in-health-and-disease-methods-and-applications/functional-mri-of-awake-behaving-macaques-using-standard-equipment>.
- Vanduffel W, Fize D, Peuskens H, Denys K, Sunaert S, Todd JT, Orban GA. 2002. Extracting 3D from motion: differences in human and monkey intraparietal cortex. *Science.* 298: 413–415.
- Vogt BA, Finch DM, Olson CR. 1992. Functional heterogeneity in cingulate cortex: the anterior executive and posterior evaluative regions. *Cereb Cortex.* 2:435–443.
- Vogt BA, Vogt L, Farber NB, Bush G. 2005. Architecture and neurocytology of monkey cingulate gyrus. *J Comp Neurol.* 485: 218–239.
- Wall MB, Smith AT. 2008. The representation of egomotion in the human brain. *Curr Biol.* 18:191–194.
- Yu CP, Page WK, Gaborski R, Duffy CJ. 2010. Receptive field dynamics underlying MST neuronal optic flow selectivity. *J Neurophysiol.* 103:2794–2807.
- Zhang T, Britten KH. 2011. Parietal area VIP causally influences heading perception during pursuit eye movements. *J Neurosci.* 31:2569–2575.